MATEC Web of Conferences **34**, 02005 (2015)
DOI: 10.1051/matecconf/20153402005

Sensitivities Of Diesel Particulate Filter Clean And Loading Models

Khamonchat Thiengkaew[1,a], Vivan Khongsup[2,b] and Ekathai Wirojsakunchai[3,c]

[1,2,3] *Department of Mechanical Engineering, Faculty of Engineering, Kasetsart University, Bangkok 10900, Thailand*

ABSTRACT. A comparison of two mathematical models from two cycle simulation software packages predicting a cold flow and filtration process of a *Diesel Particulate Filter* (DPF) is studied extensively. Three Cordierite *Diesel Particulate Filters* (DPF) models, with variations in washcoats (bare, washcoat-only, and catalyzed washcoat), are built and validated to experimental data. The goal is to estimate the values of wall permeability (k_{wall}) and friction loss coefficient (ξ) from the flow bench test and the values of soot permeability (k_{soot}) from the filtration process. Good agreements are found comparing between experimental data and simulation. The values of those parameters obtained from each software packages show the same trend among all tested DPF samples. However, they are different when comparing cases by cases because of the methodology lies in each mathematical model. **Keyword:** *Diesel Particulate Filter*, Wall Loading, Aftertreatment Cycle Simulation

1 Introduction

In present, diesel fuel is considered as one of the main energy sources in both personal and business transportations. This is due to the fact that with the same engine size, diesel engines can produce higher power and torque than gasoline engines [1] but the drawback lies in more polluted emissions, especially Particulate Matters (PM). PM or sometimes simply referred to as soot is one of the most important emission species from diesel engines. The non-homogeneous diesel combustion produces PM amounts that are order of magnitude higher than SI(Spark Ignition) engines. PM byproducts are said to be a cause of premature death, asthma, and cancer [2,3]. Diesel Particulate Filter (DPF) has been developed to collect and oxidize PM from diesel engine exhaust gases in order to solve this issue. They are installed into the exhaust system and performed like typical three-way catalytic converters in SI engines. The technology of DPF was first introduced in the early 1980's and tested for its performance on reducing PM [4] since then. With the current design of DPF, the reduction of PM from the diesel engine can be more than 95%conversion efficiency [5].

There are many literatures regarding to developing a mathematical model to study DPF's behaviors. For flow over clean DPF, Masoudi proposed on separating DPF into 8 zones which are inlet/outlet plug [6], contraction/ expansion, particulate layer, porous wall, and inlet/outlet channels, respectively. Konstandopoulas had only 5 zones that lump the Darcy term with inertial porous wall losses and neglect the effect of plug [7]. In terms of filtration processes, Konstandopoulos and Johnson first proposed the spherical unit collector concept with the diameter of d_c, and the system of multiple spherical unit collectors (or sometime referred to as a packed bed model) to describe the mechanisms through which PM is deposited on the filter substrate microstructure [8]. The changes of the filtration efficiency and pressure drop across the particulate filter porous wall, as well as the particulate deposit thickness, density, porosity, and permeability was studied. Their model was based on Kuwabara, Lee and Gieseke[9,10]. The model was later modified and outlined in Konstandopoulos [5, 11]. Currently it has been used in most of DPF simulation software packages.

Thus, the current study is aimed to investigate the 1-D model used in two distinct software packages, namely AVL-BOOST and GT-POWER for validating mathematical model with experimental data of three types of DPF. The structure of the paper is as follows. At first, the simulation setup including mathematical models of the flow-bench test and filtration process of a DPF are outlined. The simulation results from both software packages are validated with experimental data. Sensitivities of each models are compared and discussed extensively.

2 Materials and methods

2.1 Simulation setup

The specifications of tested DPF in the current study are shown in Table 1. All three filters are made of the same substrate material but have different substrate coatings. Filter A is a bare filter (no washcoat, no catalyst loadings). Filter B is washcoated only and Filter C is washcoated and loaded with Platinum (Pt). More details can be found in Wirojsakunchai [12].

[a] Corresponding author: py_dpromt@hotmail.com

Article available at http://www.matec-conferences.org or http://dx.doi.org/10.1051/matecconf/20153402005

Table 1 DPF specifications

Designation	A	B	C
Substrate	Cordierite		
Cell Density, N [CPSI]	88		
Diameter [mm]	142		
Length [mm]	152		
Substrate Volume, V_s [l]	2.44		
Wall Thickness, w_{th} [mil]	17		
Geometric Filter Area, GFA [m^2/l]	0.62		
Open Frontal Area, OFA	31%		
Washcoat	no	yes	yes
Pt Loading [g/l]	0	0	3
Substrate Porosity, Ɛ [%]	48.8	45.7	45.1
Mean Pore Diameter, d_{50} [µm]	12.8	11.8	11.8

2.2 Flow-bench test setup

The schematic of the flow-bench test apparatus is shown in Fig. 1. The system consists of an air pump drawing air through the test specimen (in this case, a DPF), a differential (U-tube) manometer measuring test pressure, an inclined manometer measuring pressure drop across the tested specimen, and thermocouples monitoring temperatures at various locations. The tested piece is attached in series with the pump and measuring equipment. A short flow straightening pipe is installed upstream of the DPF to help promote the uniform flow distribution before entering the DPF. By using air at room temperature and pressure as the working fluid, the pressure drop across a DPF was measured with in arrange of flow rates similar to the engine exhaust. A plot between pressure drop and wall filtration velocity can then be constructed.

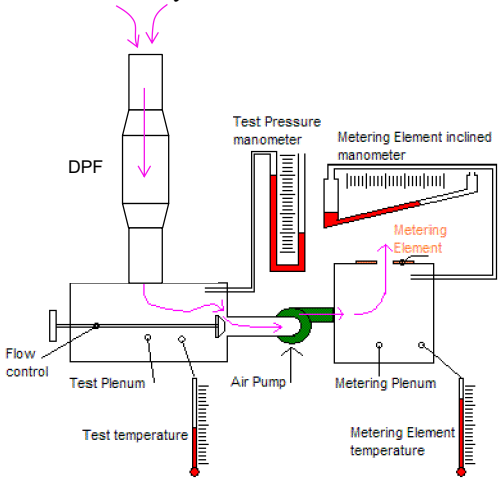

Figure 1 Schematic of the flow-bench test.

2.3 DPF loading test setup

A single-cylinder heavy-duty diesel research engine adapted from an inline six-cylinder Cummins N14-series engine was used as a PM producer in this study. The specifications of the engine are shown in Table 2. More details of this experimental setup can be found from Wirojsakunchai [13].

Table 2 Engine Tested Mode

Parameters	Value
Speed [rpm]	1800
Torque [N-m]	81
IMEP [bar]	7.3
Equivalence Ratio	0.32
Exhaust Flow Rate at DPF Inlet [kg/s]	0.051
Exhaust Temperature at Surge Tank [°C]	390
Exhaust Temperature at DPF Inlet [°C]	230
Filtration Velocity [cm/s]	5
Soot Concentration (Teflon @ 47°C) [mg/m^3]	14.5

2.4 Pressure drop model

Fig. 2 illustrates the structure of wall-flow monolith honeycomb filter which consists of many parallel channels alternatively plugged at either end. The main components inside a substrate (formed in honeycomb shape) are the inlet/outlet channel, inlet/outlet plugs, and wall filter.

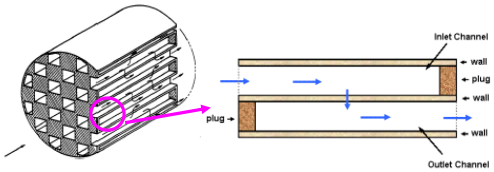

Figure 2 Schematics of the substrate of a wall-flow monolith filter and a pair of its inlet/outlet channels adapted from [5].

2.5 Flow bench test

The hydrodynamic models of the pressure drop in GT-POWER for the flow bench test are expressed in Eq. 1-6. The total pressure drop across DPF, ΔP_{clean}, is divided into 5 pressure zones as shown in Eq. 1. This model is based upon Konstandopoulas [7].

$$\Delta P_{clean}=\Delta P_{contraction}+\Delta P_{inlet,channel}+\Delta P_{wall,clean}+\Delta P_{outlet,channel}+\Delta P_{expansion} \quad (1)$$

At the inlet and outlet of the filter, changing cross sections lead to contraction and expansion effects of the flow. In order to describe additional pressure losses caused by the flow acceleration and deceleration, two correlations as shown in Eq. 2-3 are considered in the present model. They are as follows.

$$\Delta P_{contraction}=\frac{\xi_{contraction}\rho_{inlet}U_{inlet}^2}{2} \quad (2)$$

$$\Delta P_{expansion}=\frac{\xi_{expansion}\rho_{outlet}U_{outlet}^2}{2} \quad (3)$$

where the friction loss coefficient (ξ) is used to establish a quadratic relationship between the pressure drop and the inlet velocity at high flow rates.

The pressure drop due to fiction forces at the inlet/outlet channel is given by

$$\Delta P_{inlet,\,channel}=\frac{\mu Q D^2}{2V_{trap}}\frac{4FL^2}{3}\ln\left(\frac{1}{(D-2w_{wall})^4}\right) \quad (4)$$

$$\Delta P_{outlet,\,channel}=\frac{\mu Q D^2}{2V_{trap}}\frac{4FL^2}{3}\ln\left(\frac{1}{D^4}\right) \quad (5)$$

The pressure drop through clean wall filter is given by

$$\Delta P_{wall,\,clean}=\Sigma\left(\frac{\mu U_{w,\,2} w_{slab}}{k_{wall}}\right) \quad (6)$$

where the wall permeability (k_{wall}) is used to establish a linear relationship between the pressure drop and the wall velocity at low flow rates.

The hydrodynamic models of the pressure drop in AVL-BOOST for the flow bench test are expressed by Eq. 7-15. The total pressure drop across DPF, ΔP_{clean}, is divided into 8 pressure zones as shown in Eq. 7. The model is based on Masoudi[6].

$$\Delta P_{clean}=\Delta P_{effective\ filtration\ length}+\Delta P_{contraction}+\Delta P_{inlet,channel}+\Delta P_{inlet,plug}+\Delta P_{wall,clean}+\Delta P_{outlet,plug}+\Delta P_{outlet,channel}+\Delta P_{expansion} \quad (7)$$

The pressure drop over the entire effective filtration length is a solution of the calculated pressure profiles. It is given as follows.

$$\Delta P_{effective\ filtration\ length}=p_{g,1}(z=0)-p_{g,2}(z=l_{eff}) \quad (8)$$

where $p_{g,1}(z = 0)$ is the inlet channel pressure and $p_{g,2}$ ($z = l_{eff}$) is the outlet channel pressure at the beginning and end of the effective filter length.

The pressure drop due to contraction/expansion is given by

$$\Delta P_{contraction}=\frac{\xi_{contraction}\rho_{inlet}U_{inlet}^2}{2} \quad (9)$$

$$\Delta P_{expansion}=\frac{\xi_{expansion}\rho_{outlet}U_{outlet}^2}{2} \quad (10)$$

where the friction loss coefficient (ξ) is used to establish a quadratic relationship between pressure drop and the inlet/outlet velocity at high flow rates.

The pressure drop due to fiction at the entrance of the inlet and the exit of the outlet channel is given by

$$\Delta P_{inlet,channel}=\frac{1}{l_{eff}}\int_0^{l_{eff}}\left[p_{g,1}(z=0)-p_{g,1}(z)\right]dz \quad (11)$$

$$\Delta P_{outlet,channel}=\frac{1}{l_{eff}}\int_0^{l_{eff}}\left[p_{g,2}(z)-p_{g,2}(z=l_{eff})\right]dz \quad (12)$$

where the pressure difference from one position z in the filter to inlet and outlet, respectively, are evaluated and averaged over the entire effective filter length.

The pressure drop due to the fiction at the inlet/outlet plug is given by

$$\Delta P_{inlet,plug}=\varphi\mu\frac{32 l_{plug} u_{outlet}}{d_1^2} \quad (13)$$

$$\Delta P_{outlet,plug}=\varphi\mu\frac{32 l_{plug} u_{outlet}}{d_1^2} \quad (14)$$

The pressure drop through clean wall filter is given by

$$\Delta P_{wall,clean}=Vw,\,1\mu\left(\frac{\rho_{inlet}\delta_w}{\rho_{outlet}k_{wall}}\right) \quad (15)$$

where the wall permeability (k_{wall}) is used to establish a linear relationship between pressure drop and the wall velocity at low flow rates.

2.6 Loading test

The mathematical models of the filtration process in GT-POWER are expressed by Eq. 16-19. These models do not include any ash effects. The total pressure drop across DPF, $\Delta P_{Loading}$, is divided into 6 pressure zones as shown in Eq. 16.

$$\Delta P_{Loading}=\Delta P_{contraction}+\Delta P_{inlet,channel}+\Delta P_{wall,clean}+\Delta P_{outlet,channel}+\Delta P_{expansion}+\Delta P_{soot\ cake\ layer} \quad (16)$$

The pressure drop due to the inlet/outlet channel is adapted from Eq. 4 to Eq. 17 and Eq. 5 to Eq. 18. The effect from soot was added to equations given by

$$\Delta P_{inlet,channel}=\frac{\mu Q(D+w_{soot})^2}{2V_{trap}}\frac{4FL^2}{3}\ln\left(\frac{1}{(D-2w_{wall})^4}\right) \quad (17)$$

$$\Delta P_{outlet,channel}=\frac{\mu Q(D+w_{soot})^2}{2V_{trap}}\frac{4FL^2}{3}\ln\left(\frac{1}{D^4}\right) \quad (18)$$

In order to combine the effect from soot the pressure drop due to the soot cake layer is added to Eq. 1 as follows.

$$\Delta P_{soot\ cake\ layer}=\frac{\mu U_{w,1}(D-2w_{soot})}{2k_{soot}}\ln\left(\frac{D}{D-2w_{soot}}\right) \quad (19)$$

where the soot permeability (k_{soot}) is used for curve fitting between the pressure drop and the amount of soot fed to DPF.

The mathematical models of the filtration process in AVL-BOOST are expressed by Eq. 20-21. These models do not include any ash effects. The total pressure drop, $\Delta P_{Loading}$, across DPF is divided into 8 pressure zones as shown in Eq. 20.

$$\Delta P_{Loading}=\Delta P_{effective\ filtration\ length}+\Delta P_{contraction}+\Delta P_{inlet,channel}+\Delta P_{inlet,plug}+\Delta P_{wall,soot}+\Delta P_{outlet,plug}+\Delta P_{outlet,channel}+\Delta P_{expansion} \quad (20)$$

The pressure drop through clean wall in Eq. 15 is adapted because of the soot deposit effect and expressed in the term of $\Delta P_{wall,soot}$ as shown in Eq. 21.

$$\Delta P_{wall,soot}\left[v_{w,1}\mu\left(\frac{F_{nfw,A}d_1-F_{nfw,B}\delta_{sc}}{F_{nfw,A}d_1}\right)\right]\left[\frac{\rho_{inlet}}{\rho_{outlet}}\left(\frac{\delta_w}{k_{wall}}+\frac{\delta_{sd}}{k_{sd}}\right)+\frac{F_{nfw,A}d_1}{F_{nfw,B}k_{soot}}\ln\left(\frac{F_{nfw,A}d_1}{F_{nfw,A}d_1-F_{nfw,B}\delta_{sc}}\right)\right] \quad (21)$$

where the soot cake layer permeability (k_{sc}) and soot depth layer permeability (k_{sd}) is used for curve fitting between the pressure drop and the amount of soot fed to DPF.

3 Results & discussions

3.1 Flow bench test

In this section, a comparison is made between simulation and experimental data for the flow bench test. A plot between pressure drop and filtration velocity is constructed. A quadratic regression is performed based on the Darcy Forchheimer equation resulting in Permeability (k_{global}) and Contraction/Expansion coefficient (ζ) for experimental data [14] as shown in Table 3. In order to estimate the values of global permeability (k_{wall}) from Eq. 4 (using GT-POWER), Eq. 12 (using AVL-BOOST) and friction loss coefficient (ζ) from Eq. 2-3 (using GT-POWER), Eq. 9-10 (using AVL-BOOST), model tunings are performed as shown in Table 4-5. Fig. 3 depict overall filter pressure drop comparing to wall filtration velocity of Filter A, B, and C calculated by GT-POWER and AVL-BOOST, respectively.

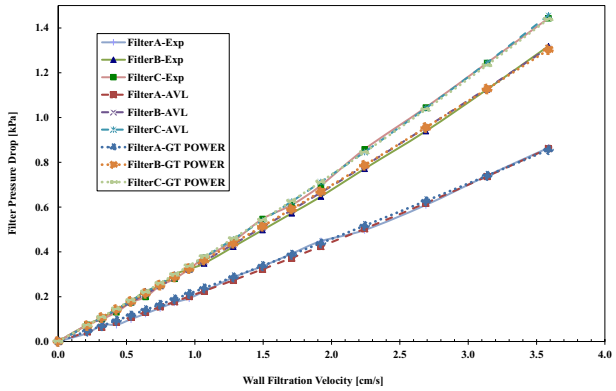

Figure 3 Filter Pressure drop vs. Filtration Velocities of Filter A, B, and C using GT-POWER and AVL-BOOST in Flow Bench Test.

As seen from Table 3-5. the value of wall permeability is reduced from filter A to C and the value of friction loss coefficient is increase from filter A to C. Adding catalyst (filter C vs. B) has slight impact on pressure drop. On the other hand, adding washcoat to a bare substrate (filter B vs. A) increases flow restriction across the wall and promotes flow losses through the contraction and expansion of the inlet and outlet channels due to the deposition of the washcoat at the corners of the square channel ceramic monolith [15].

After tuning both models, good agreements of filter pressure drop and wall filtration velocity are found between experimental data and simulation. However, if we focus on both linear and quadratic terms used in each mathematical models, the values obtained from experimental data differ from simulation because they are calibrated from different methodologies based on each models as seen in Table 3. The values of k_{global} are fitted from the Darcy term with v_{wall} (filtration wall velocity) in Darcy Forchheimer equation but the values of k_{wall} for GT-POWER and AVL-BOOST are fitted from Eq. 6 with $U_{w,2}$ (Substrate wall velocity) and Eq. 15 with $v_{w,1}$ (Wall velocity in the inlet channel), respectively. In addition, the values of ζ based on curve fitting experimental data are fitted from Forchheimer term in the same manner as k_{global} but the values of ζ for GT-POWER and AVL-BOOST are fitted from Eq. 2-3 and Eq. 9-10 with U^2_{inlet} and U^2_{outlet} (the values of inlet velocity is assumed to be the same as the outlet velocity), respectively. Due to the fact that the values of k are calibrated differently based on the velocity term used in each models, the value of ζ, even composed of the same velocity term, is therefore are not the same because it directly relates to the linear equation term in curve fitting.

Table 3 Properties of DPF Substrate from Flow Bench Experiments, GT-POWER and AVL-BOOST

	Experiments		GT-POWER		AVL-BOOST	
Filter	Permeability, (k_{global}) [m2]	Friction loss Coefficient (ζ)	Permeability, (k_{wall}) [m2]	Friction loss coefficient (ζ)	Permeability, (k_{wall}) [m2]	Friction loss coefficient (ζ)
A	3.96E-13	1.202	4.70E-13	1.950	4.65E-13	1.500
B	2.42E-13	1.514	2.85E-13	3.000	2.70E-13	1.540
C	2.37E-13	1.717	2.80E-13	5.850	2.65E-13	3.100

3.2 Loading test

In this section, a comparison is made between simulation and experimental data for filtration processes. A plot between pressure drop and soot fed to various DPF is constructed. Model tuning is performed to estimate the values of soot permeability (ksoot) from Eq. 19 for GT-POWER and Eq. 21 for AVL-BOOST. Results are shown in Fig. 4 for both GT-POWER and AVL-BOOST. The profile of the pressure drop across DPF follows the conceptual model of the filtration process as proposed by Merkel [16]. Good agreement between experimental data and simulation at wall loading (0-0.25g of soot fed) and soot cake layer loading (more than 1.5g of soot fed) stages can be found. However, during the transition stage (from wall loading to soot cake layer loading) both models fail to capture this pressure drop behavior. The reasons are described in the following paragraph.

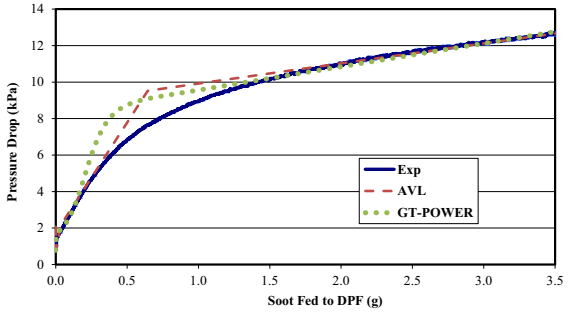

Figure 4 Filter Pressure drop vs. Soot Fed to Filter A,B(Filter C results have same trend as Filter B) from GT-POWER and AVL-BOOST.

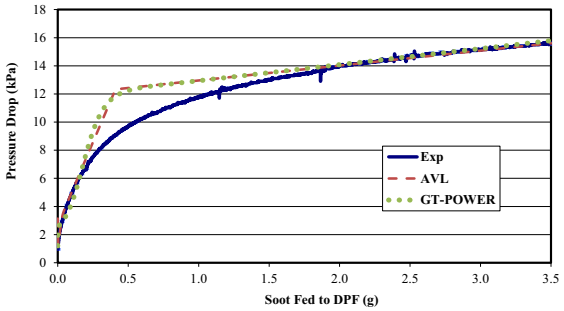

Figure 4 (Cont.)

During the transition stage, the cut point between wall loading and soot cake layer stage seen in GT-Power is much smoother than that in AVL-BOOST. GT-Power models employ a concept of a Partition coefficient, ϕ, as shown in Eq. 22 which determines the amount of particulate matter that will be deposited on the top of the filter wall before forming a soot cake layer.

$$\phi = \frac{d_{c1}^2 - d_{c0}^2}{(\Psi_b)^2 - d_{c0}^2} \tag{22}$$

The calculated Partition coefficient numerically ranges from 0-1. A value of 0 indicates that all particulates will deposit into the wall. A value of 1 indicates that all soot is being deposited as a soot cake layer. An equation of PM mass in depth filtration is given by

$$\frac{dm_{dep}}{dt} = (-K_{thm} - K_{cat}) m_{dep} + \dot{m}_{dep} \tag{23}$$

$$K = \frac{Diff \times Sh}{L_{ch}} \tag{24}$$

where K is mass transfer coefficient, Sh is Sherwood number, L_{ch} is the characteristic length (equivalent to the inverse of the area/geometric volume ratio) and Diff is the binary diffusion coefficients for the individual species in the mixture. The value of Ψ_b in Eq. 22 is the diameter of a unit collector model evolved with time which directly relates to the value of m_{dep} in Eq. 23 [17].

For the filtration model in AVL-BOOST, two distinct balance equations are applied to capture changes of soot mass in both cake and depth layer during the transition stage, which are given by

$$\frac{dm_{sd}(z)}{dt} = +\dot{R}_{sd} + v_{w,dll}(z) m_{soot,inl} S_{sd} \tag{25}$$

$$\frac{dm_{sc}(z)}{dt} = +\dot{R}_{sc} + v_{w,dll}(z) m_{soot,inl} S_{sc} \tag{26}$$

where S_{sd} is a binary switch to steer soot deposition in the depth filtration layer. Soot deposition in the depth layer (m_{sd}) is switched off as soon as sootcake is present or the depth filtration capacity is reached. The binary switch S_{sc} controls the soot deposition in the cake layer. Once S_{sd} is off and S_{sc} will be turned on as soon as the depth filtration layer has reached its full capacity. By using logic on/off in its mathematical model during the transition stage, the pressure drop profile in AVL-BOOST, therefore, does not smooth out when compared to GT-Power.

Table 4 shows the values of Soot Cake Layer Permeability (k_{soot}) and Partition coefficient (ϕ) that are tuned as shown in Fig. 4 while Table 5. shows the values of Soot Cake Layer Permeability (k_{soot}), Depth filtration threshold, and Depth filtration permeability (k_{sd}) that are tuned as shown in Fig. 4. Note that the depth filtration threshold use for switching between soot depth layer to soot cake layer.

Table 4 Properties of DPFs during Loading Simulation from GT POWER

Filter	Soot Cake Layer Permeability (k_{soot})	Partition coefficient (ϕ)
A	3.35E-15	0.9405
B	3.65E-15	0.9425
C	3.70E-15	0.9430

Table 5 Properties of DPFs during Loading Simulation from AVL BOOST

filter	Soot Cake Layer Permeability (k_{soot})	Depth filtration threshold	Depth filtration Permeability (k_{sd})
A	1.35E-14	0.3	9.5E-15
B	1.37E-14	0.19	7.7E-15
C	1.38E-14	0.19	7.66E-15

The accuracy of both transition models relies heavily on the condition for differentiating depth filtration and soot cake layer. After tuning, even both models seem to capture the pressure drop evolution during soot cake layer stage but due to the differences during the transition stage, this can cause differences in soot cake layer permeability.

4 Summary

- A 1-D model of a DPF is successfully constructed to perform the flow bench and filtration analysis in AVL-BOOST and GT-POWER.
- For flow bench test, tuning wall permeability and friction loss coefficient from both models yield similar results.
- During depth filtration and soot cake layer, both models can capture similar trends as seen in the experiment.
- However, both models show distinct results of soot cake layer permeability which is due to the transition model from which each models are based upon.

In the future study, the regeneration model will be integrated to validate with active regeneration tests in order to calibrate chemical kinetics model during regeneration process.

Acknowledgements

This work is supported by Department of Mechanical Engineering, Kasetsart University and AVL-AST Co., Ltd under AVL AST UNIVERSITY PARTNERSHIP PROGRAM.

References

1. J.B. Heywood, Internal Combustion Engine Fundamentals, McGraw-Hill, Singapore, 1988, pp. 930.
2. AVL Inc., AVL-BOOST Version 2010.1 Aftertreatment Manual, Austria, 2010, pp**.** 418.
3. N. DeNevers, Air Pollution Control Engineering, McGraw-Hill, USA, 2000, pp. 608.
4. J.H. Johnson, et al., A Review of Diesel Particulate Control Technology and Emissions Effects -1992 Horning Memorial Award Lecture, SAE International (1994), 940233.
5. A.G. Konstandopoulos, et al., Fundamental Studies of *Diesel Particulate Filters*: Transient Loading Regeneration and Aging, SAE International 2000-01-1016.
6. M. Masoudi, Hydrodynamics of *Diesel Particulate Filters*, SAE International 2002-01- 1016.
7. A.G. Konstandopoulos, Flow Resistance Descriptors for *Diesel Particulate Filters*: Definitions Measurements and Testing, SAE International 2003-01-0864.
8. A.G. Konstandopoulos, J.H. Johnson, Wall-Flow Diesel Particulate Filters-Their Pressure Drop and Collection Efficiency, SAE Technical Paper (1989) 890405.
9. S. Kuwabara, The Force Experienced by Randomly Distributed Parallel Circular Cylinders or Spheres in Viscous Flow at Small Reynolds Numbers, J. Phys. Soc. Jpn. **14**, 1959, pp**.** 527-532.
10. K.W. Lee, J. A. Gieseke, Collection of Aerosol Particles by Packed Bed, Env. Sci. Tech. **13 (4**), 1979, pp**.** 466-470.
11. A.G. Konstandopoulos, et al., Microstructural Properties of Soot Deposits in Diesel Particulate Traps, SAE International 2002-01-1015.
12. E. Wirojsakunchai, et al., Detailed Diesel Exhaust Particulate Characterization and Real-Time DPF Filtration Efficiency Measurements during PM Filling Process, SAE International 2007-01-0320.
13. E. Wirojsakunchai, The Effects of Filtration Velocities and Particulate Matter Characteristics on *Diesel Particulate Filter* Wall Loading Performance, Ph.D. Thesis, UNIVERSITY OF WISCONSIN-MADISON, USA, 2008, pp. 215.
14. E. Wirojsakunchai, Validation of a 3D Model for Predicting Pressure Drop of a Clean *Diesel Particulate Filter*, The 23rd Conference of the Mechanical Engineering Network of Thailand, Thailand, 2009.
15. R.M. Heck, et al., Catalytic Air Pollution Control: Commercial Technology, John Wiley&Sons Inc., New York, 2002, pp. 522.
16. G.A. Merkel, et al., New Cordierite Diesel Particulate Filters for Catalyzed and Non-Catalyzed Applications, Proceedings of the 9th Diesel Engine Emissions Reduction Conference, USA, 2003.
17. A.G. Konstandopoulos, et al., Progress in Diesel Particulate Filter Simulation, SAE International 2005-01-0946.
18. P. Eastwood, Particulate Emissions from Vehicles, John Wiley&Son Ltd., The Atrium, Southern Gate, Chichester, West Sussex P0198SQ, England, 2008, pp. 493.
19. Gamma Technologies, GT-POWER Version7.1 Exhaust Aftertreatment Application Manual, USA, 2010, pp. 32.